Electric Motor Noise from Small Quadcopters: Part I – Acoustic Measurements

Dennis L. Huff[1] and Brenda S. Henderson[1]
NASA Glenn Research Center, Cleveland, Ohio, 44135

There is increased interest in using electric motors to drive propulsors across a range of small air vehicle classes. Applications include both vertical lift and conventional takeoff and landing systems for Small Unmanned Aircraft Systems. Mission profiles call for integrating these systems into urban airspaces exposing populated areas to new noise sources. In addition to the propulsor noise from rotors and propellers, electric motors are expected to contribute to the overall sound levels and possibly human annoyance. This work presents acoustic measurements of electric motors used for small quadcopters to characterize the sound and identify sources with and without a propeller. Free field microphone measurements were used to determine directivity and a phased microphone array was used to identify sound sources. A companion paper (Part II – Source Characteristics and Prediction) compares the far field results with current probe measurements of the signal driving the motor, the structural response of the motor case, and describes prediction methods of electric motor noise.

I. Introduction

Electric motors are being used for small Unmanned Aircraft Systems (sUAS) across a wide range of sizes and applications. The motors drive propellers that are known to be noisy as sUAS fly over populated areas on the ground. There has been an increase in the number of sUAS operating in the airspace with demand that is expected to significantly grow. There are plans to use sUAS for package deliveries to residential locations.[1] There are also visions of utilizing vertical lift vehicles for transporting people for on-demand mobility (ODM) in urban areas.[2] For both of these applications it will be important to address noise issues by identifying noise sources, applying noise reduction technologies, and developing prediction methods that can be used to evaluate their impact on community noise.

Vertical lift "quadcopters" use four motors to drive propellers with variable speed control. While most of the noise from a sUAS comes from the propeller, there is evidence that a portion of the noise also comes from the electric motors.[3,4] Sound spectra show that tones from the electric motor can dominate in frequency bands around 4 to 6 kHz, which are important for perceived noise levels for human hearing and annoyance. A primary source for this noise is the vibration of the case enclosing the rotor, stator and magnets of the motor. For the small quadcopters, the outer case rotates and the stator is inside the motor. The case is exposed to the air and the sound can freely radiate from each motor.

The purpose of this work is to study the noise from small quadcopter electric motors. Several motors were tested both in isolation and with a propeller for various speeds to measure acoustic directivity. A phased microphone array was used to help identify sound sources. A current probe was used to measure the signal from the speed controller to the motor for comparisons with the acoustic spectra. A complementary paper[5] focuses on structural analysis of the case and the prediction of the frequencies that contribute to the sound field. Casing resonance vibration modes and loading on the motor cause an amplification of tones and can become a dominant noise source.

A longer term objective of this work is to develop noise prediction methods for a wide range motor sizes that can be used in aircraft noise prediction codes, such as NASA's Aircraft Noise Prediction Program (ANOPP). The current work with small motors is an initial cost-effective step to document source mechanisms and develop noise prediction methods. Future work will focus on larger motors that will be used on air vehicles using either batteries or turbo-electric power sources.

Research Aerospace Engineer, Acoustics Branch, MS 54-3, AIAA Associate Fellow.

II. Experimental Approach

Acoustic tests were done in the Acoustic Testing Laboratory (ATL) at the NASA Glenn Research Center (Figure 1). The ATL is an anechoic chamber with a cut-off frequency of 100 Hz. The interior dimensions of the chamber are 21-ft. deep x 17-ft. wide x 17-ft high. The ATL has a removable steel grate working platform and access to portable floor wedges to convert the facility into a hemi-anechoic chamber.

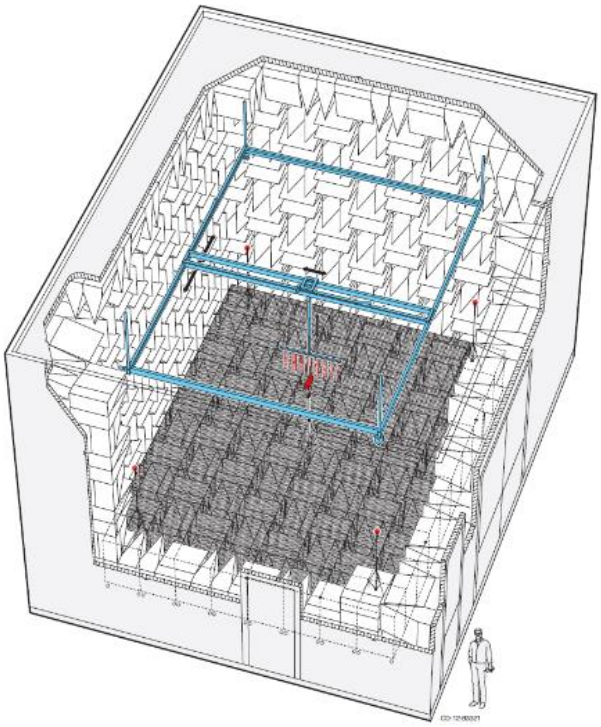

(a)

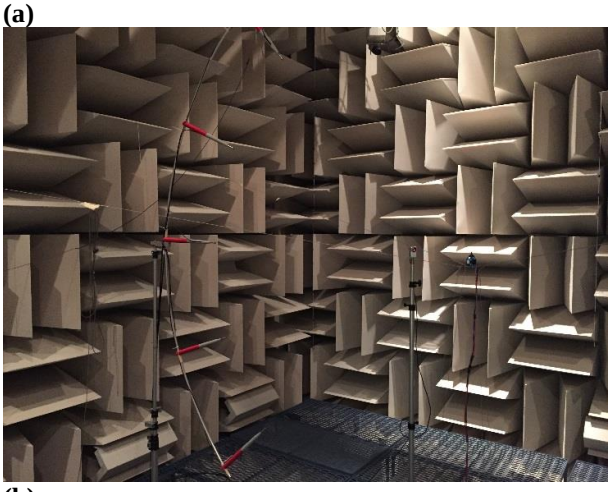

(b)

Figure 1. Acoustic Test Laboratory (ATL) at the NASA Glenn Research Center. (a) Schematic. (b) Picture of ATL with motor and microphone array.

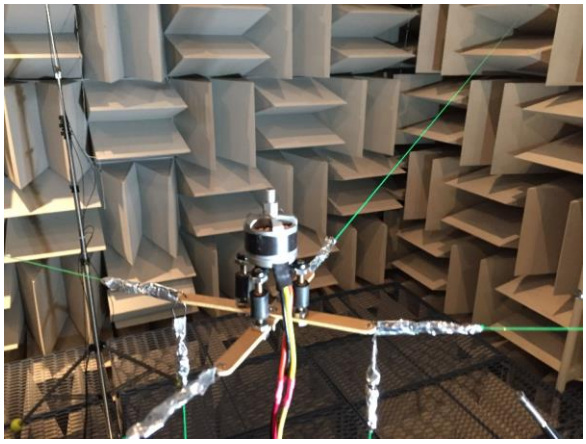

Figure 2. Method for mounting motor in ATL

Initial tests mounted the motors on a pole cantilevered from the floor. A vibration damping coupler was used to minimize structural excitations to the mount, however, this was shown to not work very well due to unwanted sound coming from the cantilevered pole. Tests were also conducted with the motor hanging from a ceiling traverse using its electronic control wires and strings. This was found to be best for minimizing extraneous mounting noise, but was difficult to control the motor orientation relative to microphone arrays due to the motor torque. Finally, a mounting fixture was constructed using wood craft sticks and nylon fishing line to suspend the motor in the middle of the chamber. Two sticks were attached in a cross and tied taught to the tips of several acoustic wedges on the walls. Swivel connectors were used and taped to minimize vibrations. Vertical lines were used to fix the height, which was especially important when propellers were mounted that created an upward force. A close-up of the motor mount is shown in Figure 2.

Three arrays of microphones were used to measure the free-field acoustics (Figure 3(a)). Each array contained five microphones on a constant radius arc. The arrays are designated small, medium and large, and had an arc radius, R, of 10, 40 and 75-inches, respectively. The center microphone on each array was oriented 90-degrees from the motor shaft axis, which is the direction normal to the motor case. There were two microphones below and two microphones above the center microphone to measure the directivity of noise. Figure 3(b) shows a picture of the installation viewed from the right rear side of ATL looking toward the motor. Figure 3(c) through Figure 3(e) shows the directivity angles for each array.

In addition to the free-field microphone arrays, a phased microphone array was used to help identify extraneous noise sources, and distinguish sources between the propeller and motor case. The phased array was an ACAM 100 manufactured by the Signal Interface Group with BeamformX software written by OptiNav, Inc..[6] The array was placed one meter away from the motor case at various locations surrounding the motor. It was determined that

positioning the array normal to the motor case (90-degrees) provided the best assessment of noise originating from the motor. Figure 4 shows the phased microphone array installed in ATL.

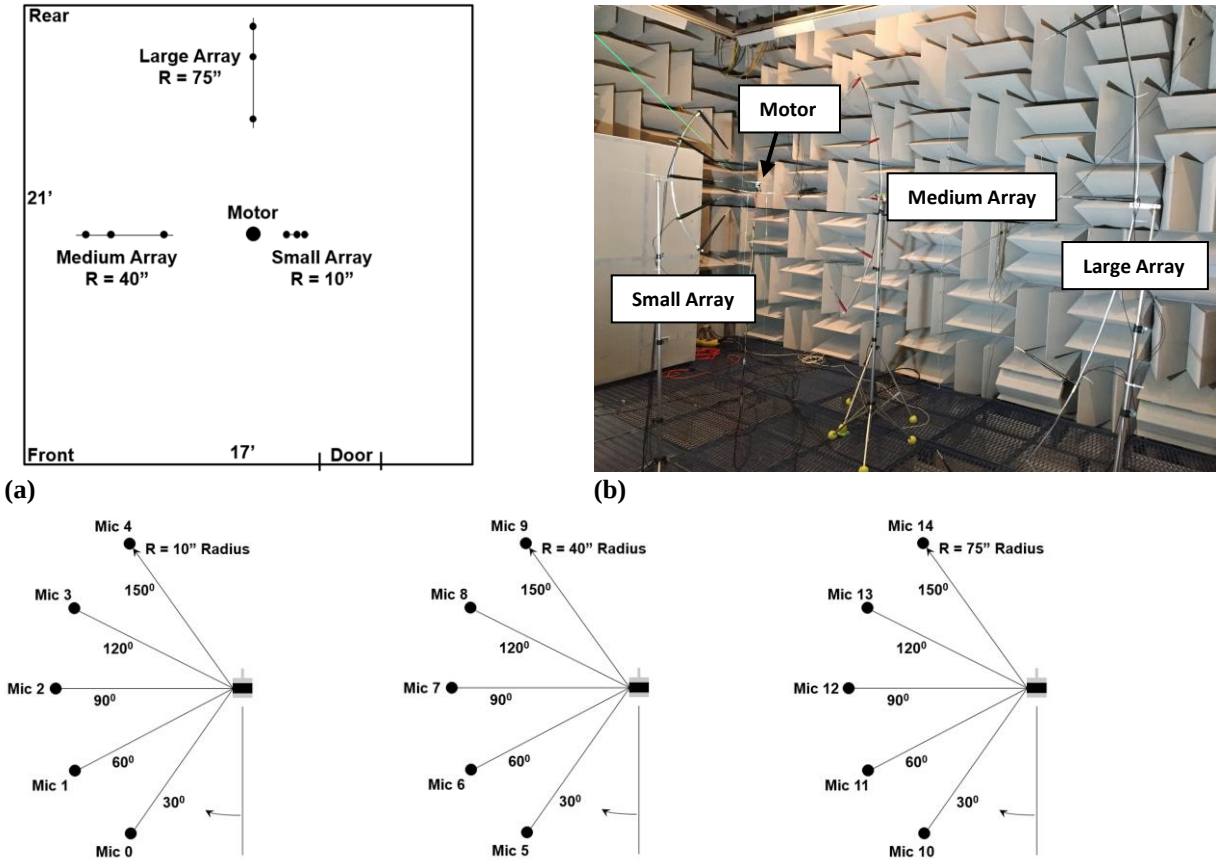

Figure 3. Microphone arrays. (a) Top view schematic in ATL. (b) Arrays installed in ATL. (c) Small. (d) Medium. (e) Large.

In addition to the acoustic measurements, the motor speed was simultaneously recorded using an optical laser probe. The laser was mounted on a tripod and pointed at the rotating motor case. The case was painted black and a strip of reflective tape was added to generate the once-per-rev signal from the optical probe. A Tektronix TCP-303 probe was used to record the current in one of the three wires leading from the speed controller to the motor. The results from the current probe measurements are included in the companion paper.[5]

Figure 4. Phased microphone array in “Front Normal” position.

III. Results

A summary of the test matrix is shown in Figure 5. Three motors that are commonly used in small quadcopters were tested over several speeds that are representative of typical operating conditions. The model numbers of the motors were 3DR (850 kV), 2212 (920 kV), and 2312 (960 kV). All three motors have 14 magnetic poles and 12 stators. Three speed controllers were used with each motor. The speed controllers were designated E300, 3DR and 420S. The E300 and 3DR controllers use square wave inputs to control the speed, where the 420S uses a sine wave. They were investigated to study the impact on noise. The results are presented in the companion paper.[5] The loading on the motors was varied by testing the motor only, and adding two- and three-bladed propellers. For all tests, the free field acoustics and phased microphone array were used to characterize the sound field. An accelerometer was placed on the motor rotor case for static ping tests to determine casing structural natural frequencies and damping levels.

	3DR "Blue"	2212	2312
Speed Variation (RPM)	4380, 5370, 6260	4380, 5370, 6260, 4773	4380, 5370, 6260, 4773
Acoustics (Small, Medium, Large Arrays)	X	X	X
Speed Controllers			
E300	X	X	X
3DR	X	X	-
420S	-	X	X
Load			
Motor Only	X	X	X
2-Bladed	X	X	X
3-Bladed	-	-	X
Phased Array	X (location study)	X	X
Current Probe	2 loops	1 loop	1 loop
Ping Test	X	X	X
Motor kV Constant (1/Ke)	850	920	960

Figure 5. Test matrix.

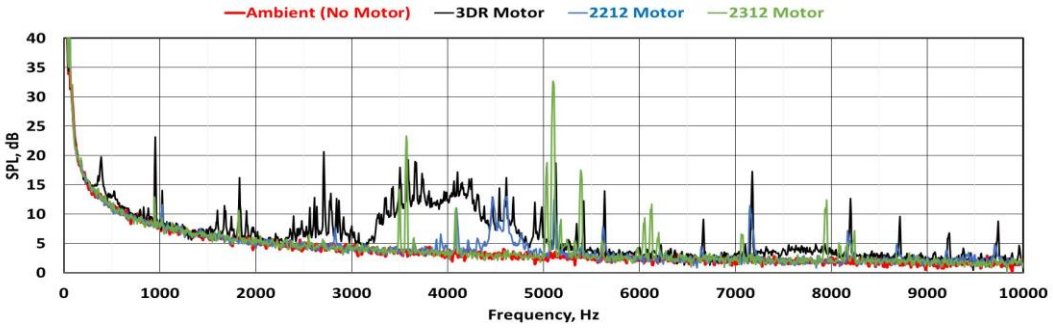

Figure 6. Background noise and motor only SPL comparisons for three motors, microphone 9 on medium array, 4380 RPM.

A comparison of the ambient sound pressure level (SPL) spectra with motor only data are shown in Figure 6. All three motors are plotted for the upper microphone (microphone 9) on the medium microphone array. The ambient levels represent the limit of the ¼-inch microphones rather than the true background noise in ATL. The spectra from the motors are for the lowest speed tested (4380 RPM) and without a load (motor only). The spectra from each motor have different characteristics for tones and broadband levels, but they all show sufficient signal-to-noise levels to distinguish tones above the background levels, and broadband noise levels over frequencies ranging from 2000 to 5500 Hz

Sample directivity SPL spectra are shown in Figures 7 through 9 for the 3DR, 2212 and 2312 motors, respectively. The medium array was used for these plots with microphone 8 data removed due to inconsistencies with this channel. All three motors show dominant radiation of sound in a direction normal to the motor case (toward microphone 7) over most frequencies, with the levels falling off above and below the motors at other angles. For the 3DR motor (Figure 7), there is a broadband noise peak that radiates above the motor towards microphone 9 from about 3000 to 4500 Hz and below the motor towards microphone 5 from about 3000 to 4000 Hz. For the 2212 and 2312 motors, the dominant radiation of sound is normal to the motor case (microphone 7) across all frequencies.

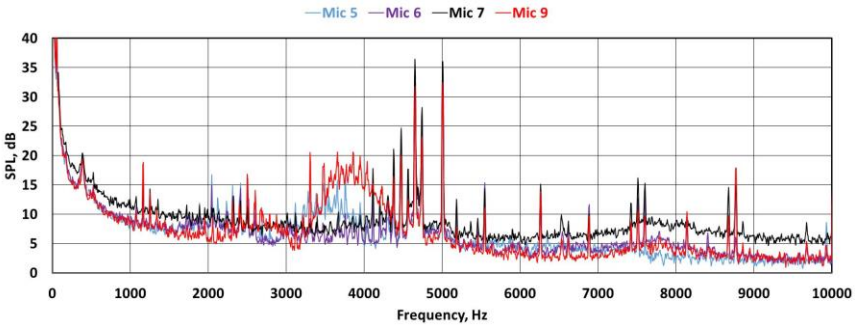

Figure 7. SPL directivity on medium array for 3DR motor, 5370 RPM, motor only.

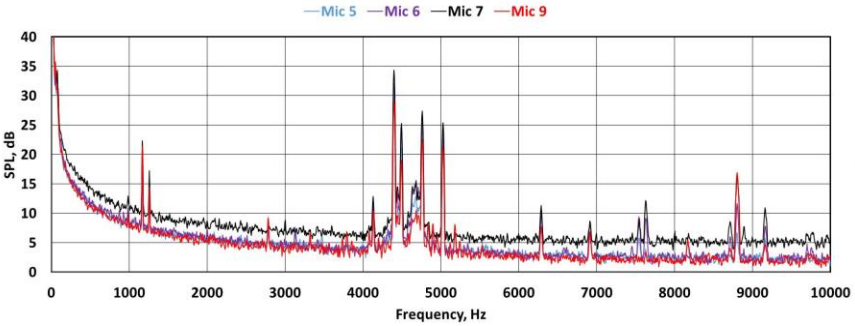

Figure 8. SPL directivity on medium array for 2212 motor, 5370 RPM, motor only.

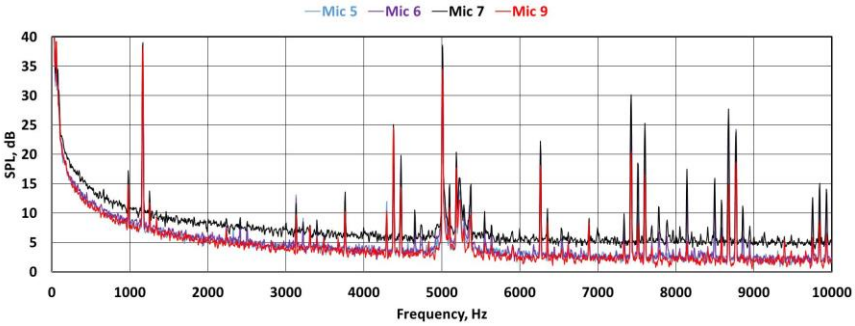

Figure 9. SPL directivity on medium array for 2312 motor, 5370 RPM, motor only.

The influence of loading on the radiated noise is explored next. Figure 10 shows the SPL spectra for the 3DR motor using the 3DR controller driving the motor at 5370 RPM. Figure 10(a) is for motor only and Figure 10(b) applies a load using a two-bladed propeller. Adding the propeller introduces blade passing frequency tones and higher harmonics that are evident up to about 4000 Hz. At this speed, the shaft order frequencies occur at multiples of 89.5 Hz. Every other harmonic (multiples of 179 Hz) contain harmonics of blade passing frequencies from the two-bladed propeller. The tones from the propeller have a higher amplitude than the shaft order tones up to about 5000 Hz. The propeller also increases the broadband noise across the entire spectra. The directivity of sound reverses the trend from motor only results with peak levels above (microphone 9) and below the motor (microphone 5). This is consistent with acoustic data presented in Ref. 3 using a similar motor. Two tones associated with the motor at 4651 and 5011 Hz (Figure 10(a)) are amplified by the propeller loading by about 10 to 15 dB (Figure 10 (b)). Figure 11 shows SPL directivities for selected frequencies of the narrowband spectra shown in Figure 10. The amplification of the motor tones and the directivity trends with and without the propeller are evident in these plots.

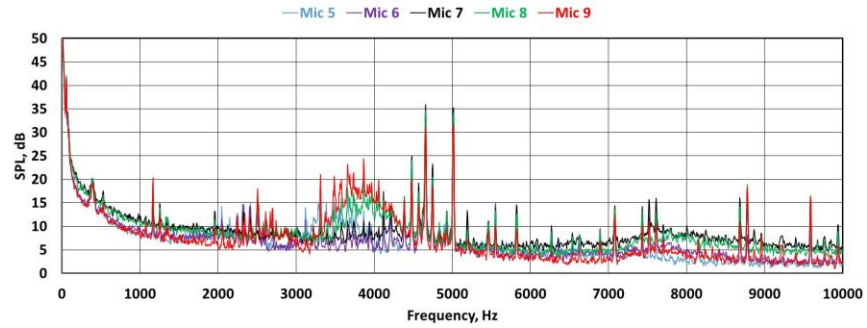

(a)

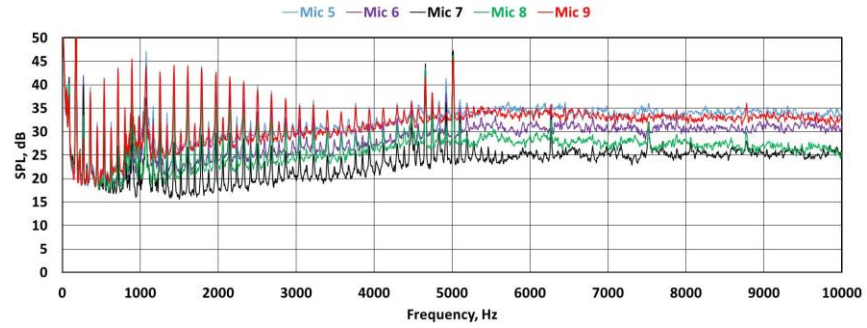

(b)

Figure 10. SPL spectra on medium array for 3DR motor, 5370 RPM. (a) Motor only. (b) Two-bladed propeller and motor.

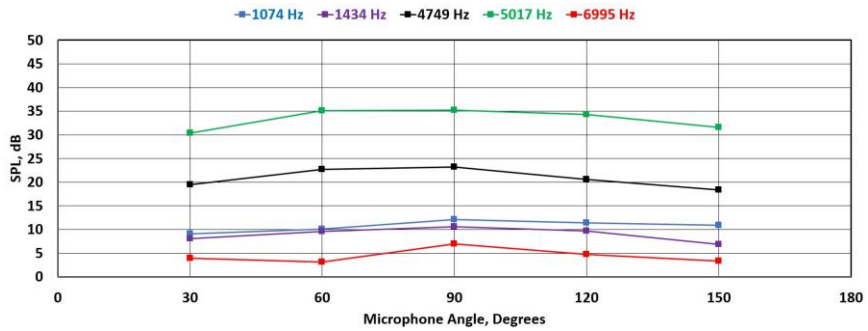

(a)

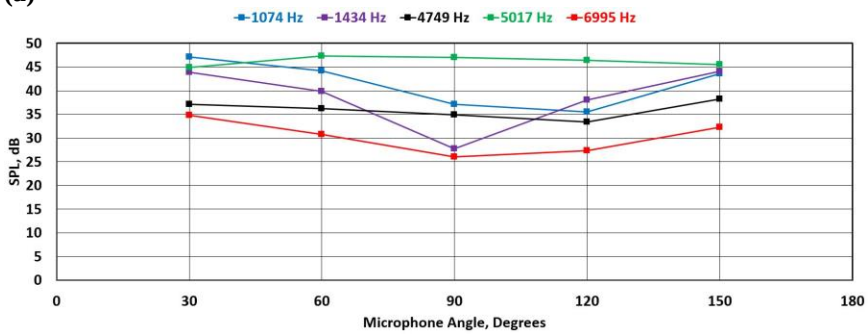

(b)

Figure 11. SPL directivity for selected frequencies on medium array for 3DR motor, 5370 RPM. (a) Motor only. (b) Two-bladed propeller and motor.

The phased microphone array was used to help locate the noise sources across the acoustic spectra. In order to confirm that the phased array could be used to isolate tones, a simulation was done where specific tones were emitted from small speakers placed on a pedestal and separated by a distance similar to the distance between the motor case and the tip of the propeller. The results are not shown here, but were found to be satisfactory for frequencies ranging from 4000 to 6300 Hz where the motor tones were observed.

The placement of the phased array was also studied for the 3DR motor running at 5370 RPM with and without the two-bladed propeller. Figure 12 shows the SPL spectra processed from the phased array with a 48.8 Hz bandwidth and comparing phased array positions relative to the motor. For all cases the phased array is located normal to the motor case and centered in the plane of rotation of the motor case (Figure 12(b)). The "rear normal" position faces the motor from the rear of ATL at a distance of 39 inches. The "front normal" position is located at the same distance but position at the front of ATL (Figure 3(a)).

The results plotted in Figure 12 show qualitative similarity in spectra at the front and rear positions of the phased array, but quantitative differences over some range of frequencies, such as below 4000 Hz for motor only spectra. However the two tones at 4639 and 5030 Hz from the motor show similar results at both positions. The tone amplification that was observed from the propeller loading using the medium array microphones is also observed in the phased array results.

Figure 13 shows similar SPL spectra from the phased array located radially 34-inches below the motor as shown in the photograph (Figure 13(b)). The directivity of the sound is consistent with the medium array free field measurements showing stronger propeller tones below the motor. For all positions of the phased array in Figures 12 and 13, the motor tones have the highest SPL across the spectra even with the propeller. Since the focus of this work is on electric motor noise, the "normal" position of the phased array was used for subsequent measurements.

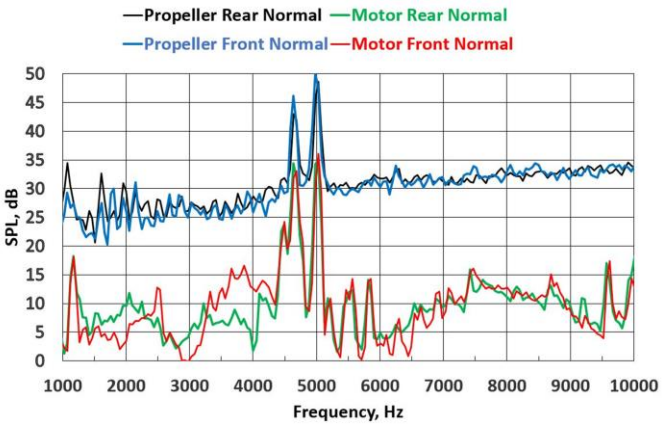

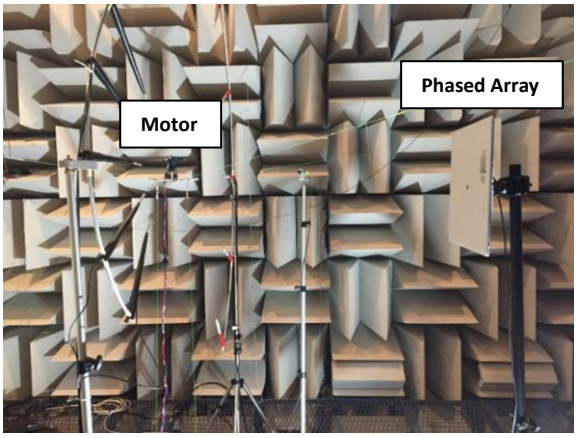

(a) **(b)**

Figure 12. Phased array spectra for 3DR motor, 5370 RPM. (a) SPL. (b) Position of phased array *normal* to the motor.

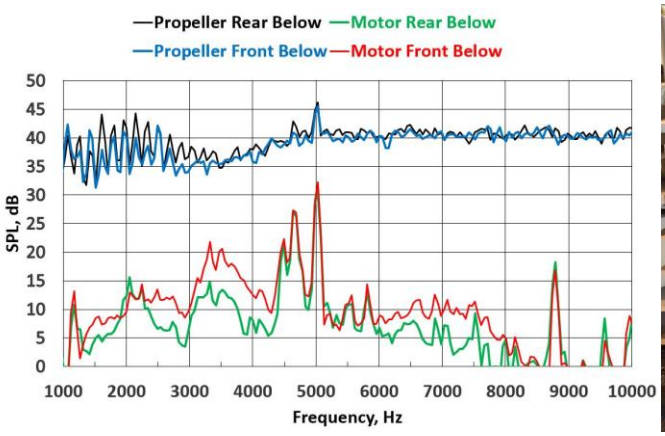

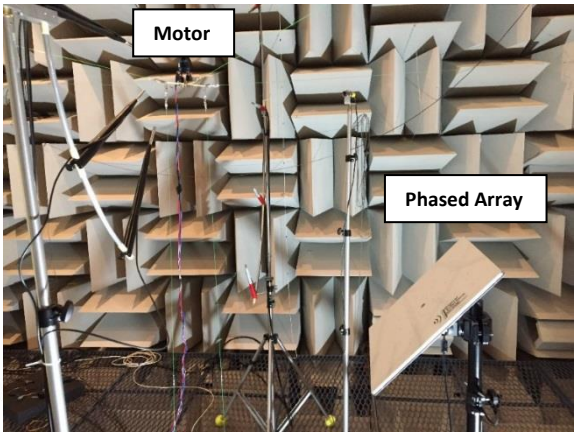

(a) **(b)**

Figure 13. Phased array spectra for 3DR motor, 5370 RPM. (a) SPL. (b) Position of phased array *below* the motor.

Comparisons of the medium array, microphone 7 spectra, and the phased array spectra for the 3DR motor at 5370 RPM are shown in Figures 14 and 15 for motor only and with a propeller, respectively. Note that the microphone 7 data was processed with a 6.10 Hz bandwidth and the phased array spectra used 48.8 Hz. The spectra for both cases are in good agreement when accounting for the different bandwidths. In Figure 15 there is about a 10 dB increase in SPL for frequencies associated with the propeller noise, which is probably due to the distributed source across the blades and the different bandwidths. The amplification of the motor tones is evident at 4639 and 5030 Hz. There are also motor tones being amplified at 6250 and 7519 Hz.

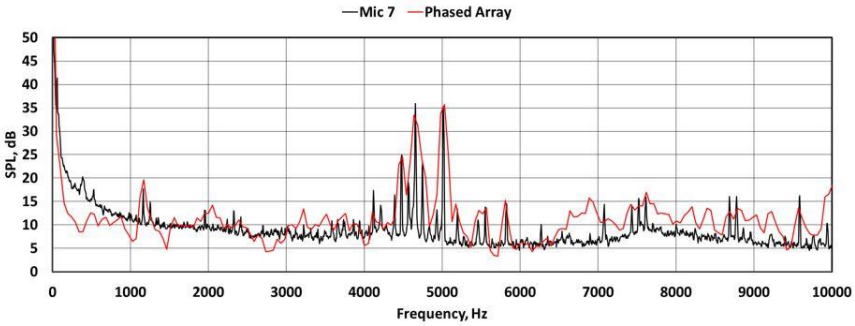

Figure 14. SPL comparisons for microphone 7 versus phased array, 3DR motor, 5370 RPM,

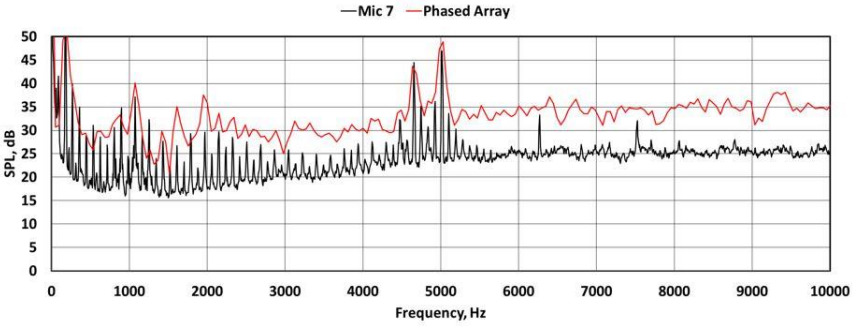

Figure 15. SPL comparisons for microphone 7 versus phased array, 3DR motor, 5370 RPM, propeller.

Images from the beamforming of the phased microphone array are shown in Figures 16 through 23 for discrete frequencies of 1172, 2050, 4638, 5029, 5469, 6250, 7520 and 7617 Hz, respectively. The images and plots on the left side of the figures are for motor only, and the images and plots on the right side are for cases with a propeller. The tone at 1172 Hz for motor only is shown in Figure 16(a) to originate near the right side of the motor case. Adding the propeller causes the source to shift to the propeller (Figure 16(b)). The source is shifted toward the advancing side of the propeller blades. (The propeller rotates clockwise viewed from the top, so the blade is advancing on the right side of the propeller in the pictures). A similar result is shown in Figure 17 for 2050 Hz, but the propeller source is more distributed across the top and bottom of the blade. The resolution of the phased array becomes an issue below about 1000 Hz, so the results at higher frequencies should be reliable.

Figures 18 and 19 show the spectra and imaging for the two tones attributed to the motor. The beamforming results support that the motor case is the source of the tones with or without the propeller. The images show the source is centered on the right side of the case for 4638 Hz and shifts to the right side of the case for 5029 Hz.

Figure 20 is for 5469 Hz and shows a clear separation between the motor only, where the noise originates from the motor case (Figure 20 (a)), and when the propeller is added, where the sound radiates from the tip of the propeller (Figure 20(b)). In Figures 21 and 22, the sound source with a propeller appears to come from a combination of the propeller and the motor case, where the sound for motor only clearly comes from the motor case. This suggests that the propeller load is amplifying the contribution from the motor source. Finally, Figure 23 shows a clear separation of sources again at 7617 Hz between the motor and the propeller.

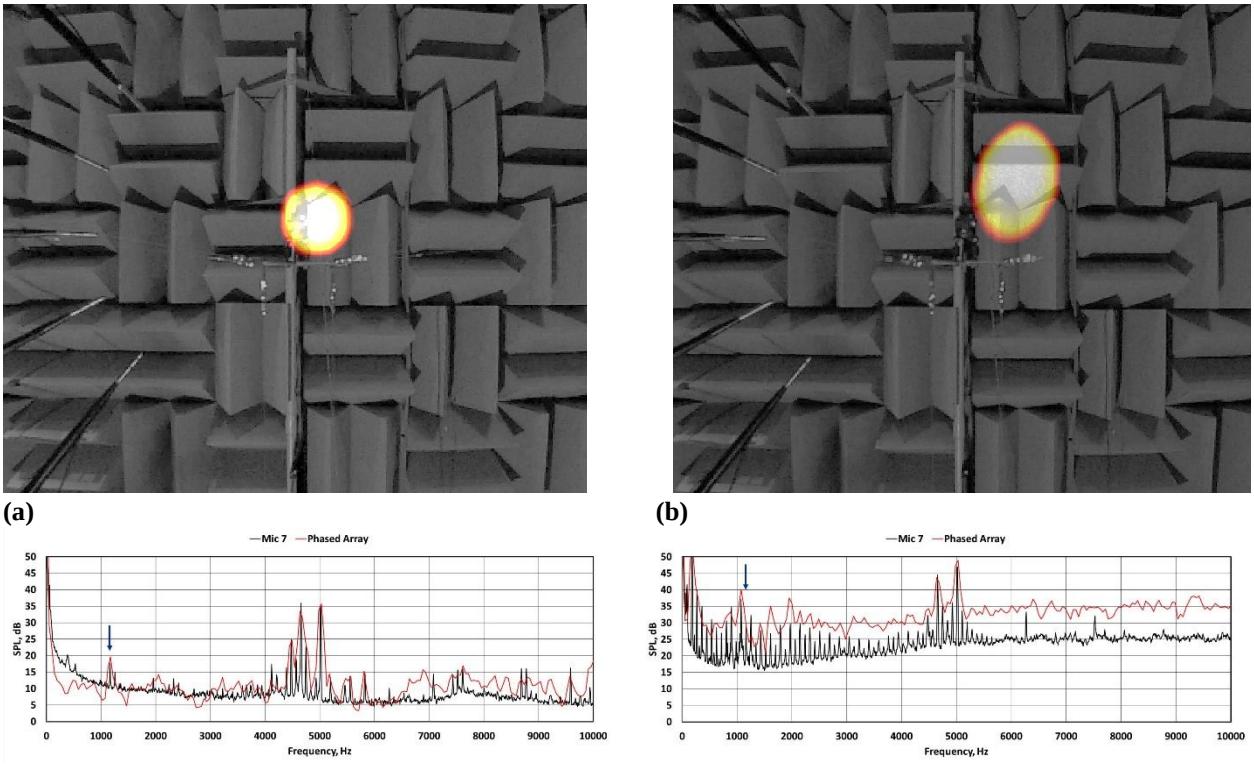

Figure 16. Phased array data for 3DR motor, 5370 RPM, 1172 Hz (blue arrow in SPL). (a) Beamform image for motor only. (b) Beamform image for propeller. (c) SPL for motor only. (d) SPL for propeller.

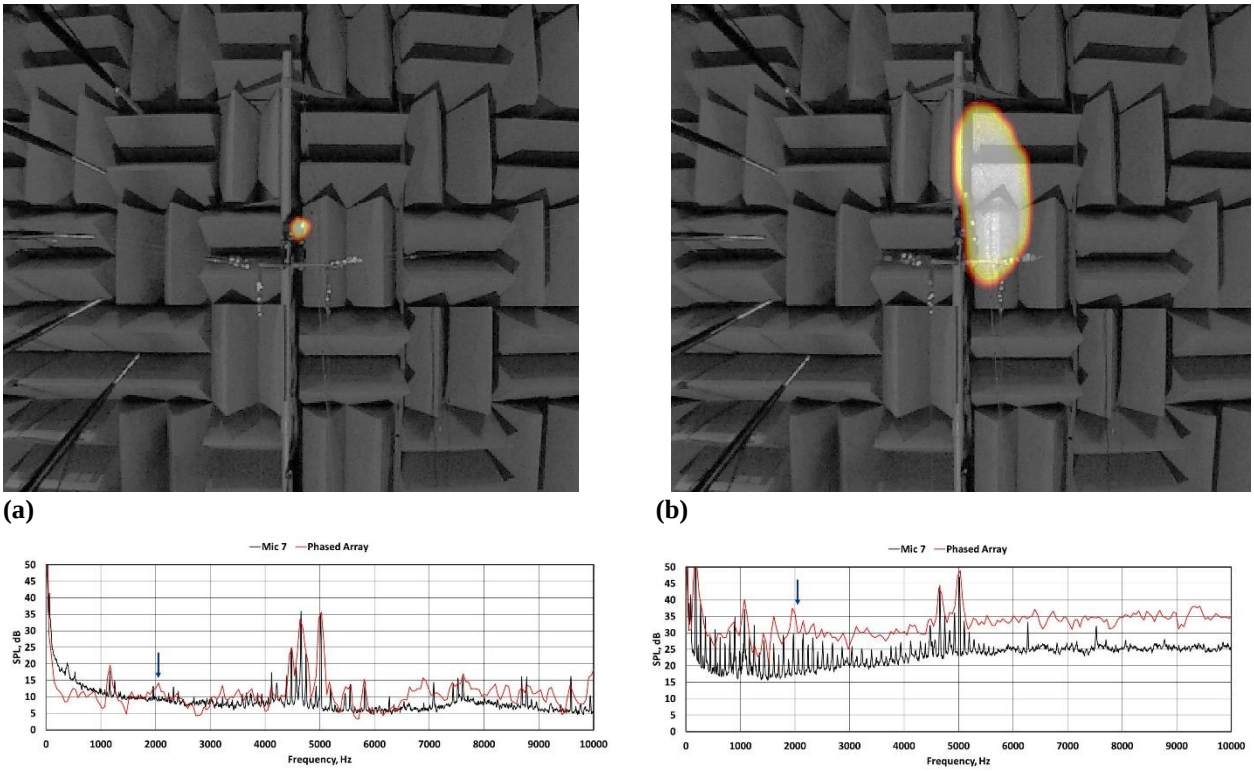

Figure 17. Phased array data for 3DR motor, 5370 RPM, 2050 Hz (blue arrow in SPL). (a) Beamform image for motor only. (b) Beamform image for propeller. (c) SPL for motor only. (d) SPL for propeller.

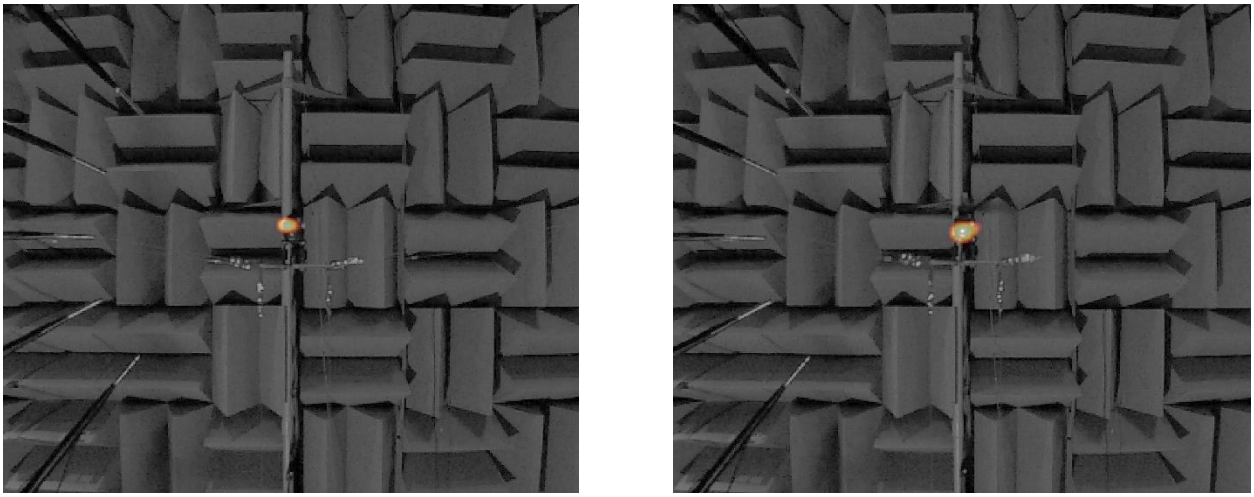

(a) (b)

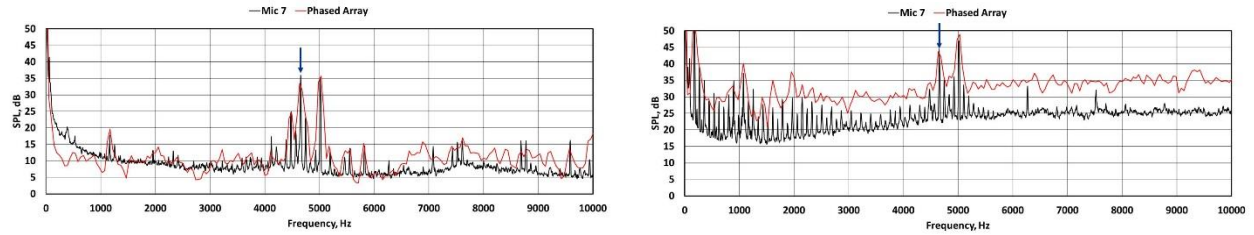

(c) (d)

Figure 18. Phased array data for 3DR motor, 5370 RPM, 4638 Hz (blue arrow in SPL). (a) Beamform image for motor only. (b) Beamform image for propeller. (c) SPL for motor only. (d) SPL for propeller.

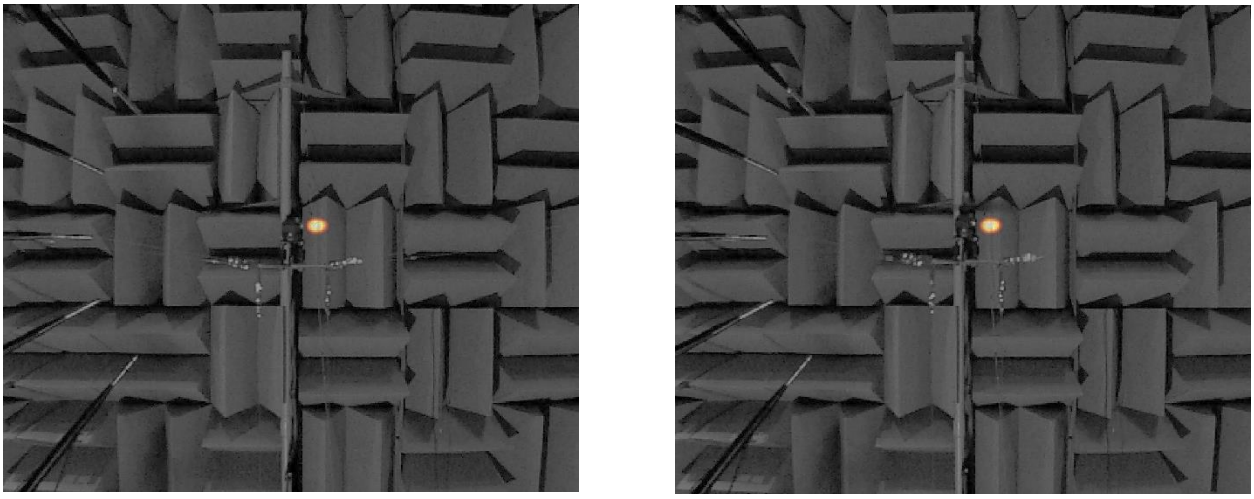

(a) (b)

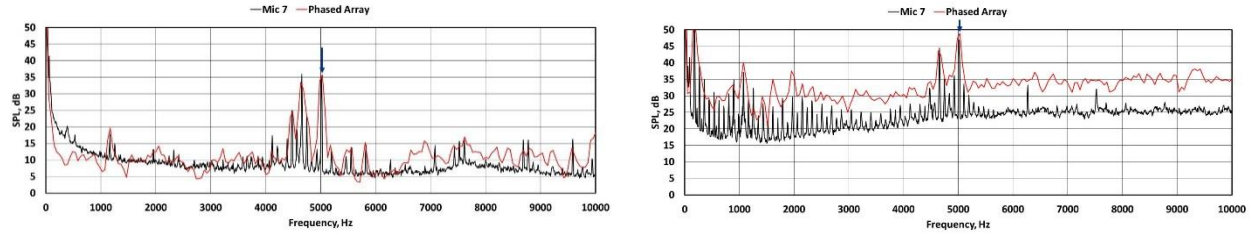

(c) (d)

Figure 19. Phased array data for 3DR motor, 5370 RPM, 5029 Hz (blue arrow in SPL). (a) Beamform image for motor only. (b) Beamform image for propeller. (c) SPL for motor only. (d) SPL for propeller.

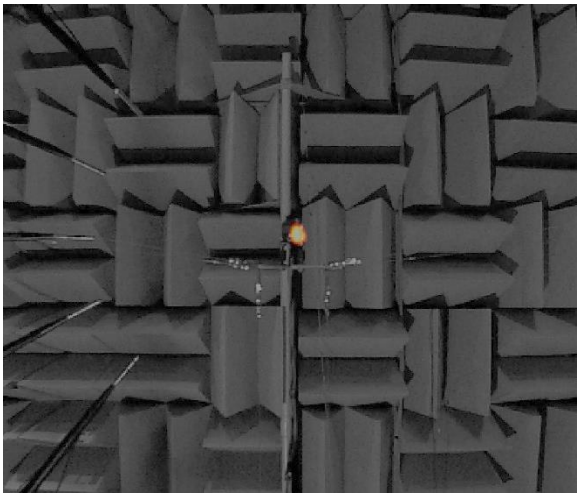

(a)

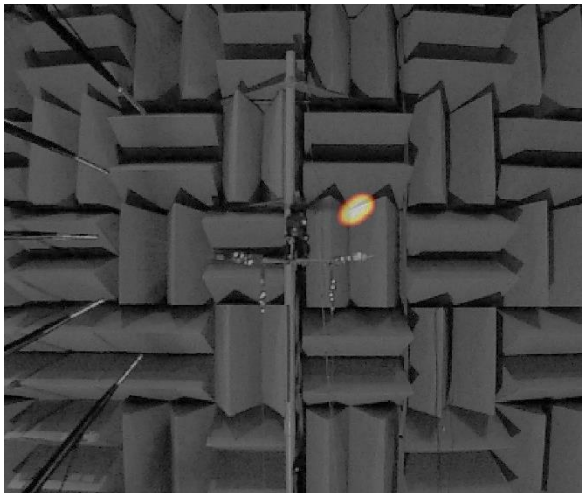

(b)

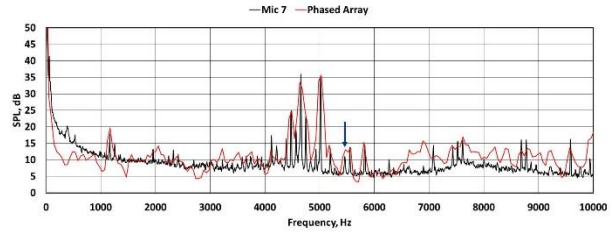

(c)

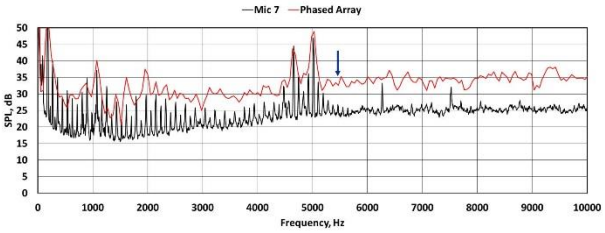

(d)

Figure 20. Phased array data for 3DR motor, 5370 RPM, 5469 Hz (blue arrow in SPL). (a) Beamform image for motor only. (b) Beamform image for propeller. (c) SPL for motor only. (d) SPL for propeller.

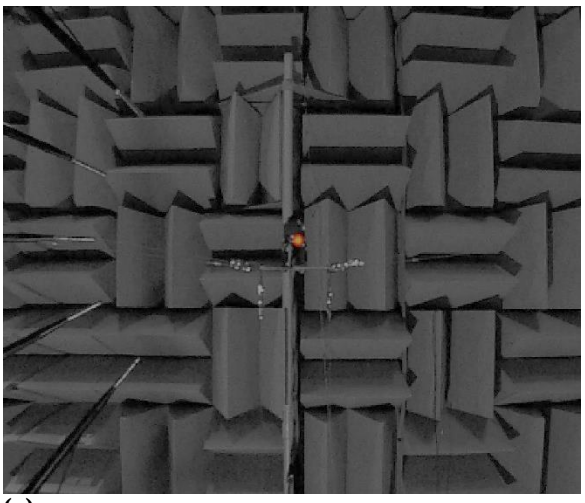

(a)

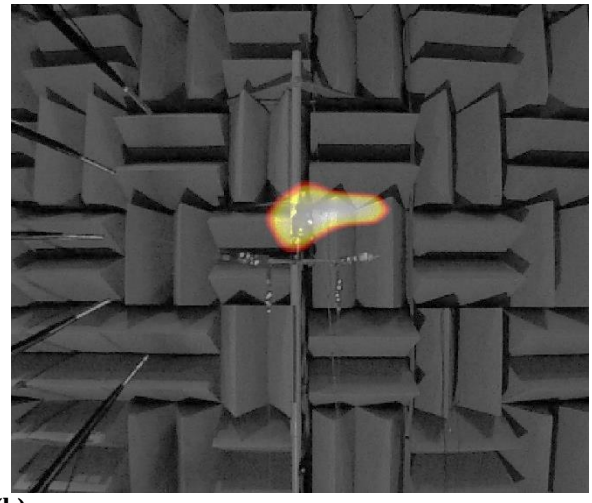

(b)

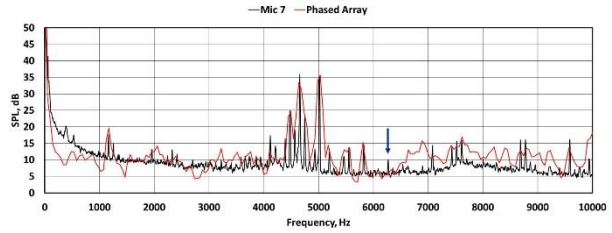

(c)

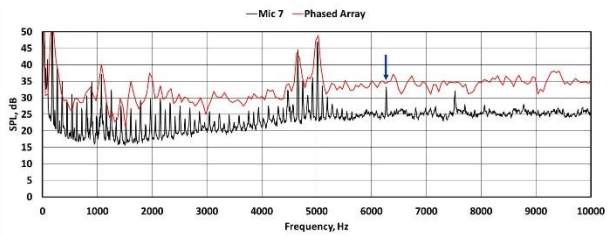

(d)

Figure 21. Phased array data for 3DR motor, 5370 RPM, 6250 Hz (blue arrow in SPL). (a) Beamform image for motor only. (b) Beamform image for propeller. (c) SPL for motor only. (d) SPL for propeller.

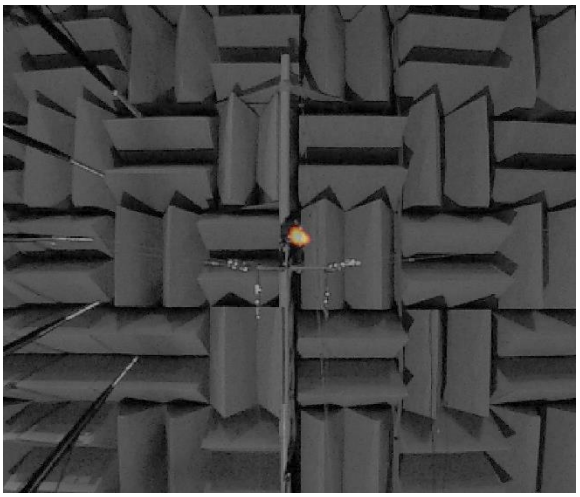

(a)

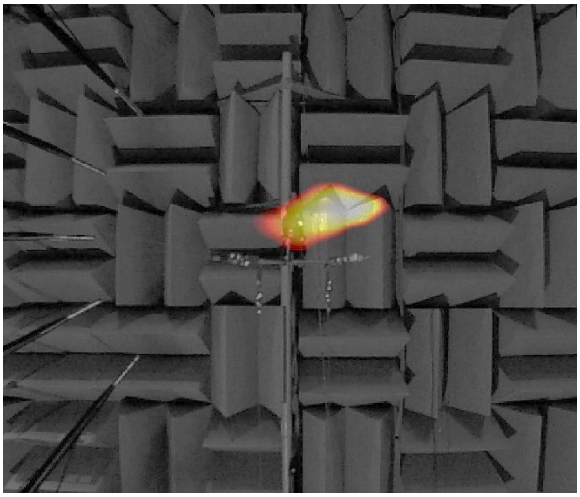

(b)

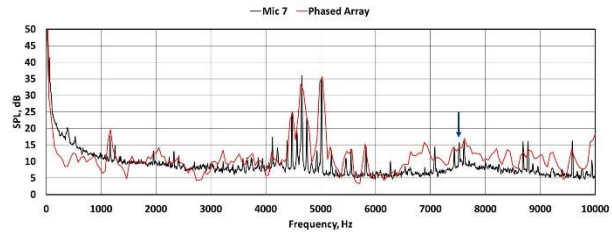

(c)

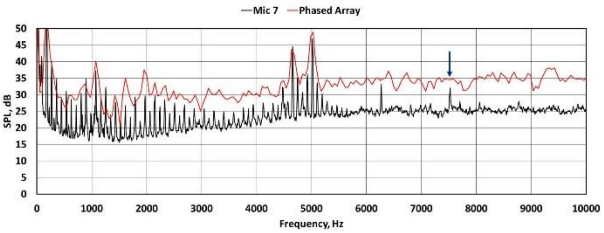

(d)

Figure 22. Phased array data for 3DR motor, 5370 RPM, 7520 Hz (blue arrow in SPL). (a) Beamform image for motor only. (b) Beamform image for propeller. (c) SPL for motor only. (d) SPL for propeller.

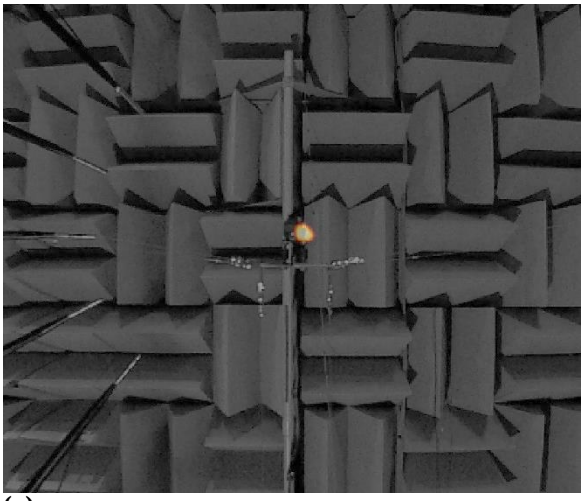

(a)

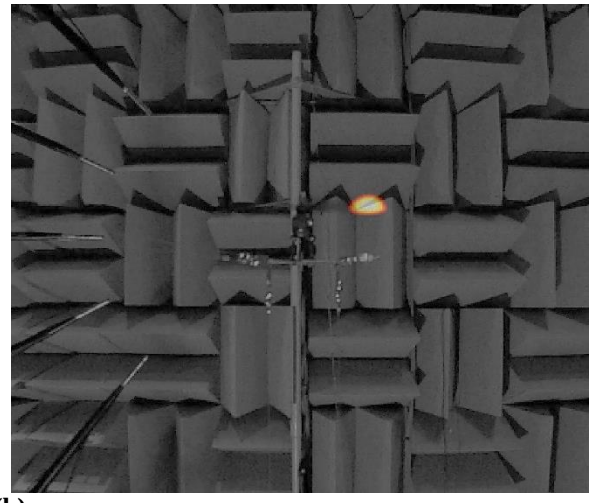

(b)

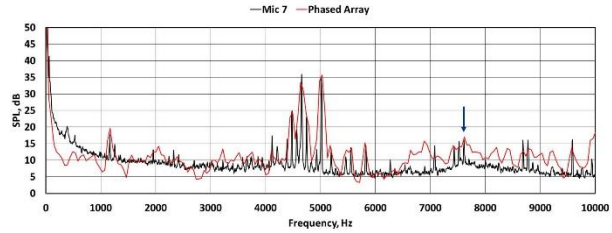

(c)

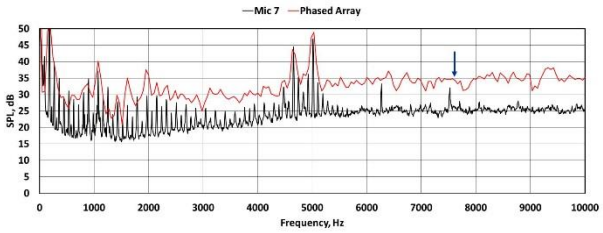

(d)

Figure 23. Phased array data for 3DR motor, 5370 RPM, 7617 Hz (blue arrow in SPL). (a) Beamform image for motor only. (b) Beamform image for propeller. (c) SPL for motor only. (d) SPL for propeller.

Similar data were acquired for the 2312 motor with 2-bladed and 3-bladed propellers (Figure 24). Comparisons of the medium array, microphone 7 spectra, and the phased array spectra for the 2312 motor at 5370 RPM are shown in Figures 25, 26 and 27 for motor only, a 2-bladed propeller and a 3-bladed propeller, respectively. The amplification of the motor tones is evident for the two-bladed propeller as it was for the 3DR motor, but the increase in SPL is less (~5 dB). The three-bladed propeller did not appear to amplify the motor tones and propeller noise becomes most important.

Images from the beamforming of the phased microphone array are shown in Figures 28 through 33 for discrete frequencies of 3125, 4394, 5029, 5224, 6250, and 6885 Hz, respectively. The narrow range of frequencies were selected to focus on the motor noise. The weak tone at 3125 Hz for motor only is overcome by propeller noise for both two and three blades (Figure 28). For 4394 Hz, the 2-bladed propeller appears to have contributions from both the motor and the propeller (Figure 29). Once the 3-bladed propeller is used, the contribution from the motor is reduced. The strongest motor tone occurs at 5029 Hz (Figure 30). The motor remains the primary source of noise with both propellers at this frequency. The tone at 5224 Hz (Figure 31) shows relative contributions similar to 4394 Hz. For higher frequencies at 6250 Hz (Figure 32) and 6885 Hz (Figure 33), both propellers dominate over the motor.

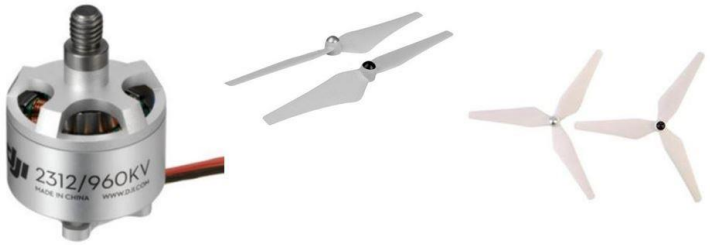

(a) (b) (c)

Figure 24. Load conditions. (a) 2312 motor. (b) 2-bladed "9443" propeller. (c) 3-bladed "9450" propeller.

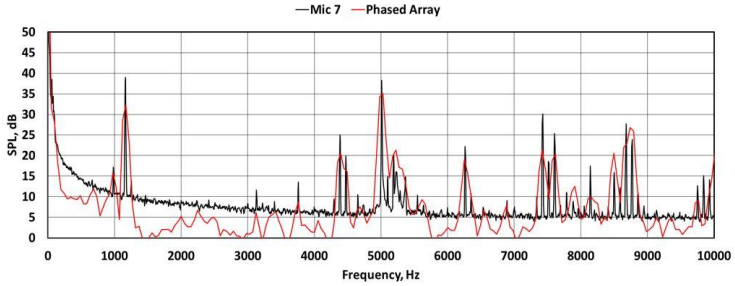

Figure 25. SPL comparisons for microphone 7 versus phased array, 2312 motor, 5370 RPM, motor only.

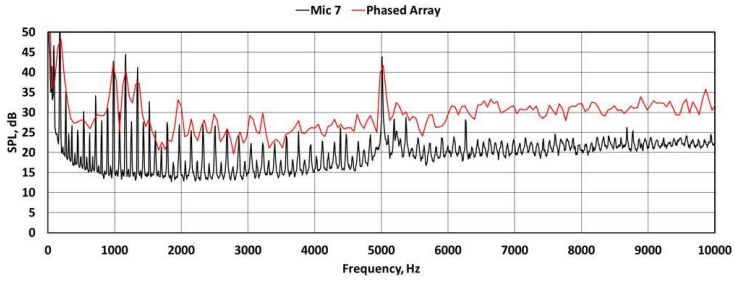

Figure 26. SPL comparisons for microphone 7 versus phased array, 2312 motor, 5370 RPM, 2-bladed propeller.

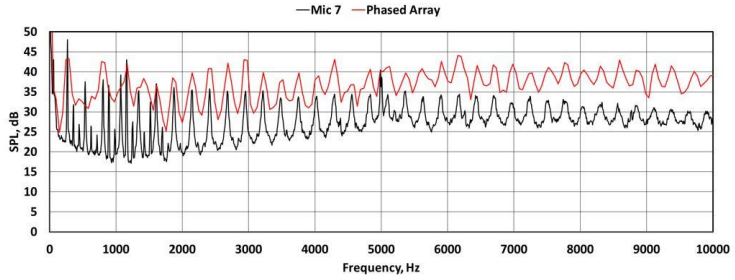

Figure 27. SPL comparisons for microphone 7 versus phased array, 2312 motor, 5370 RPM, 3-bladed propeller.

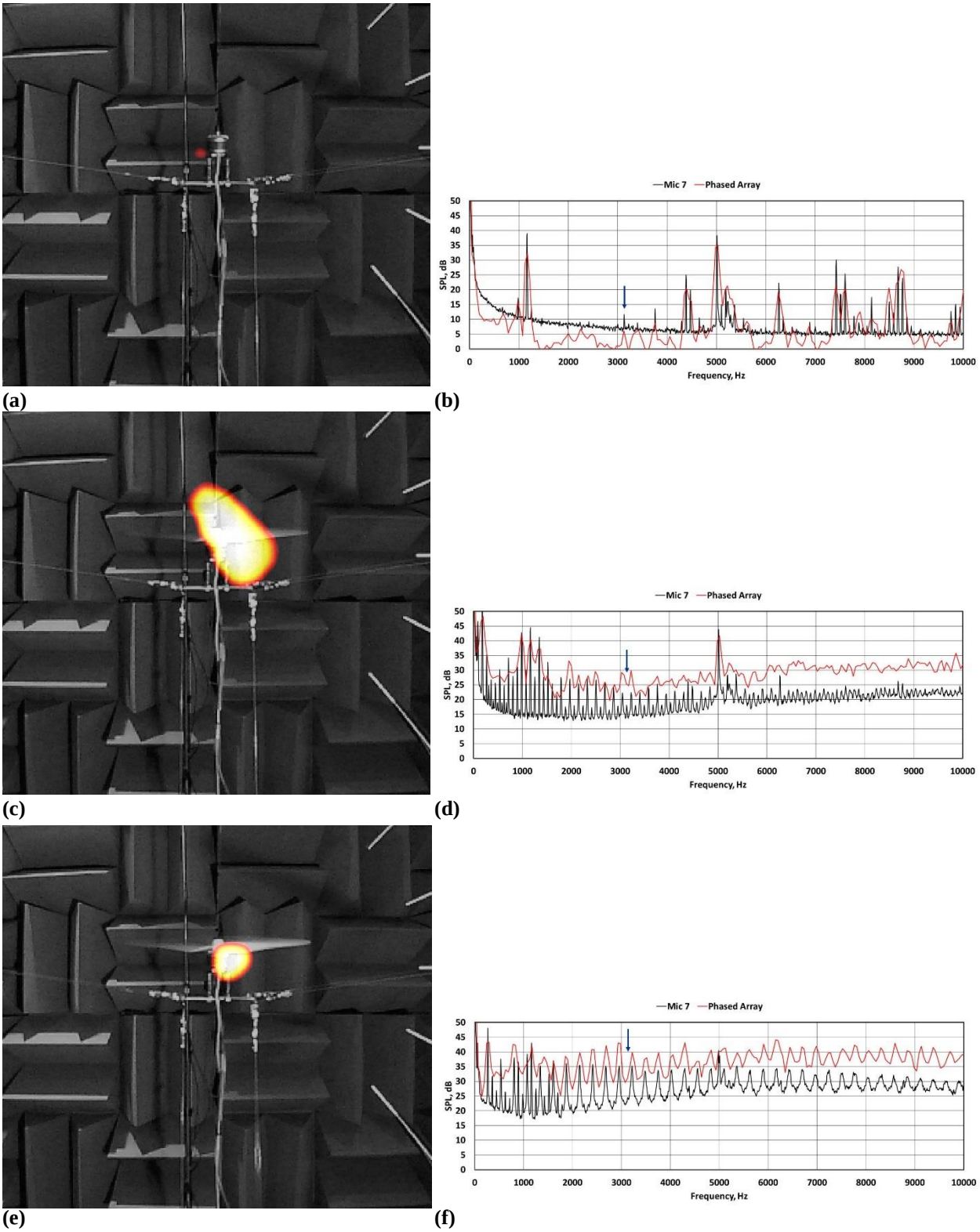

Figure 28. Phased array data for 2312 motor, 5370 RPM, 3125 Hz (blue arrow in SPL). (a) Beamform image for motor only. (b) SPL for motor only. (c) Beamform image for 2-bladed propeller. (d) SPL for 2-bladed propeller. (e) Beamform image for 3-bladed propeller. (f) SPL for 3-bladed propeller.

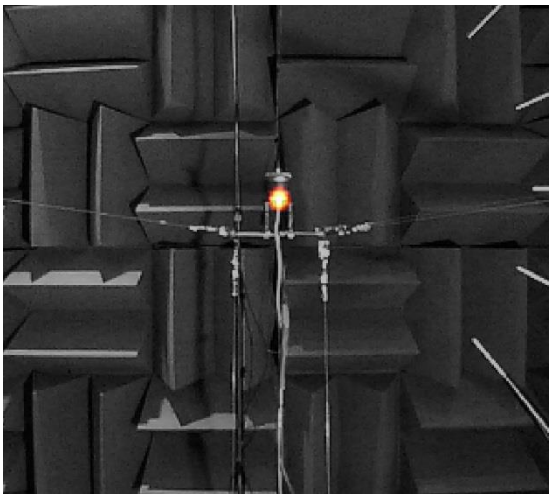

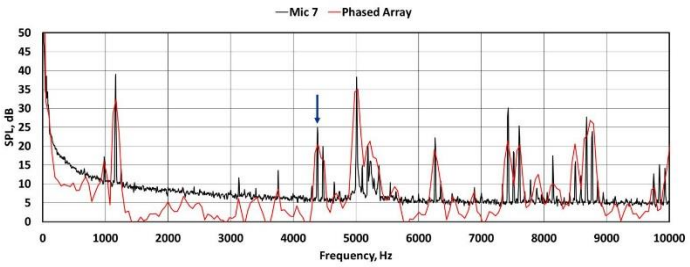

(a) (b)

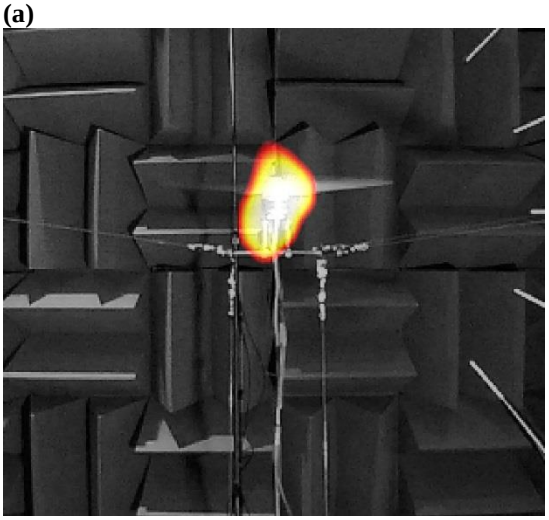

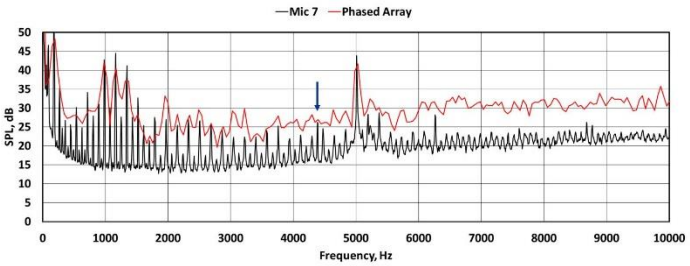

(c) (d)

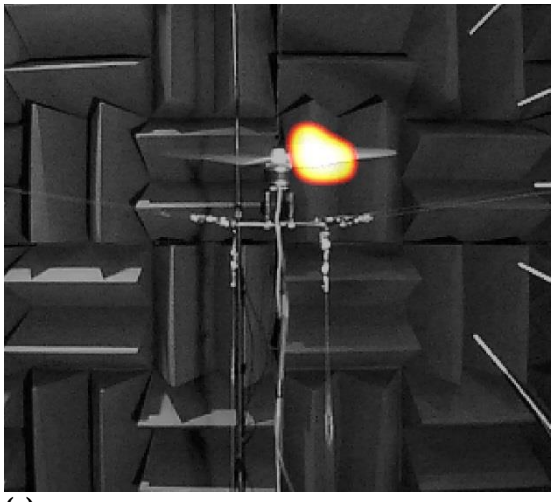

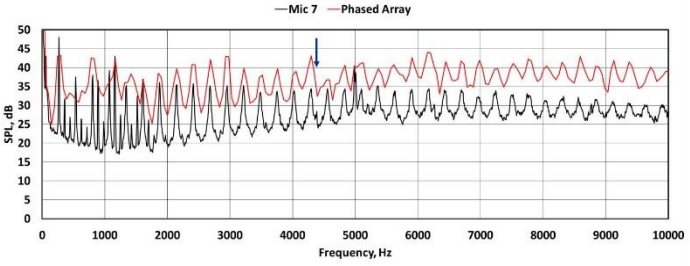

(e) (f)

Figure 29. Phased array data for 2312 motor, 5370 RPM, 4394 Hz (blue arrow in SPL). (a) Beamform image for motor only. (b) SPL for motor only. (c) Beamform image for 2-bladed propeller. (d) SPL for 2-bladed propeller. (e) Beamform image for 3-bladed propeller. (f) SPL for 3-bladed propeller.

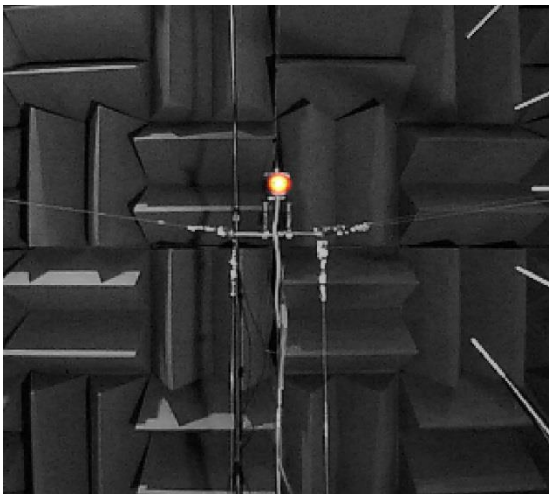

(a)

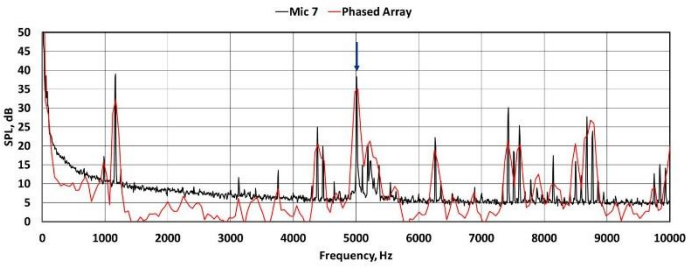

(b)

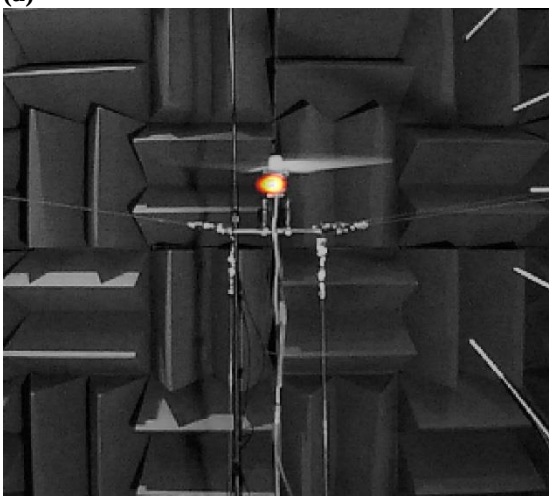

(c)

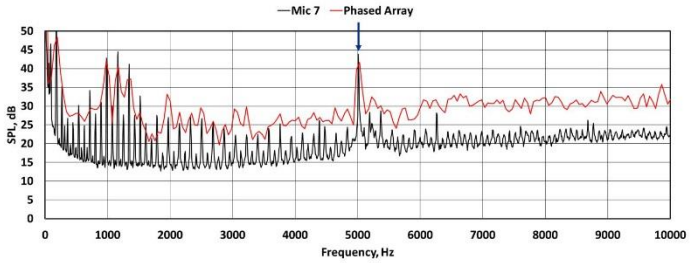

(d)

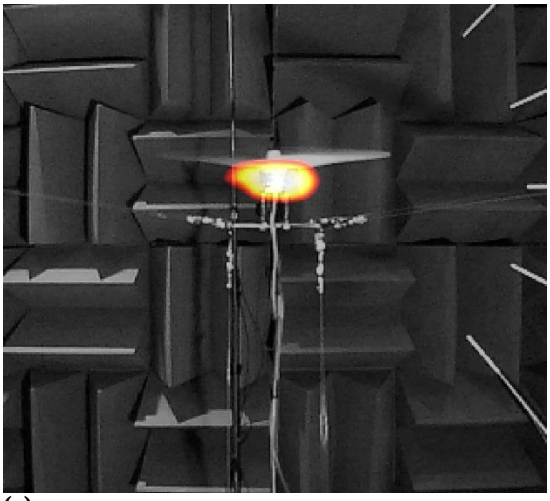

(e)

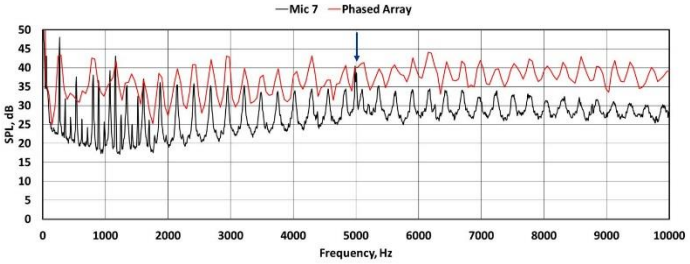

(f)

Figure 30. Phased array data for 2312 motor, 5370 RPM, 5029 Hz (blue arrow in SPL). (a) Beamform image for motor only. (b) SPL for motor only. (c) Beamform image for 2-bladed propeller. (d) SPL for 2-bladed propeller. (e) Beamform image for 3-bladed propeller. (f) SPL for 3-bladed propeller.

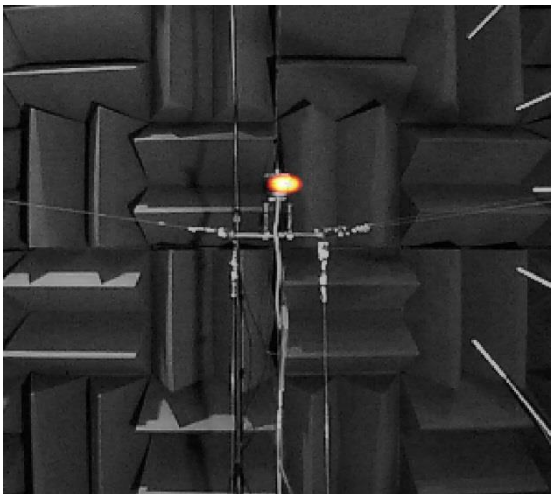

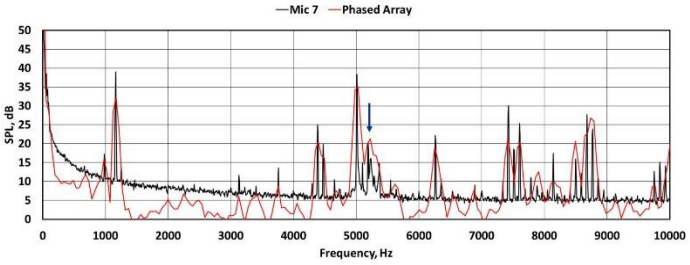

(a) **(b)**

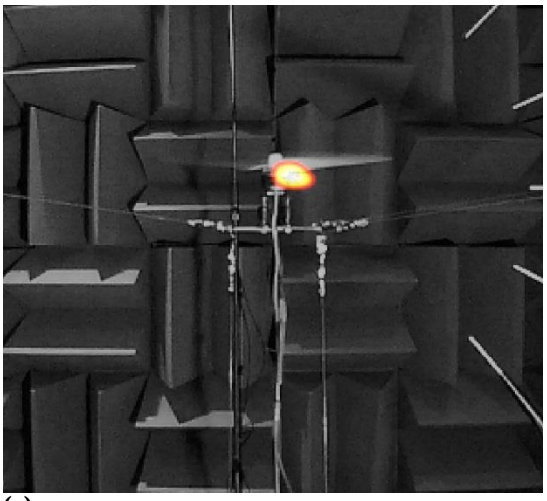

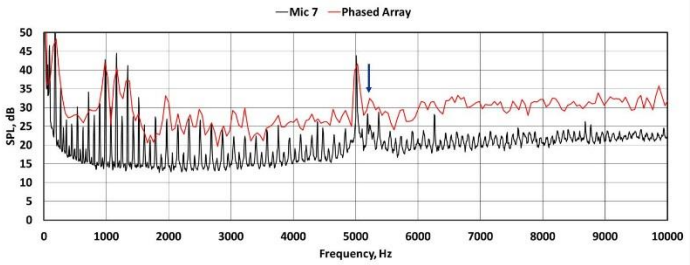

(c) **(d)**

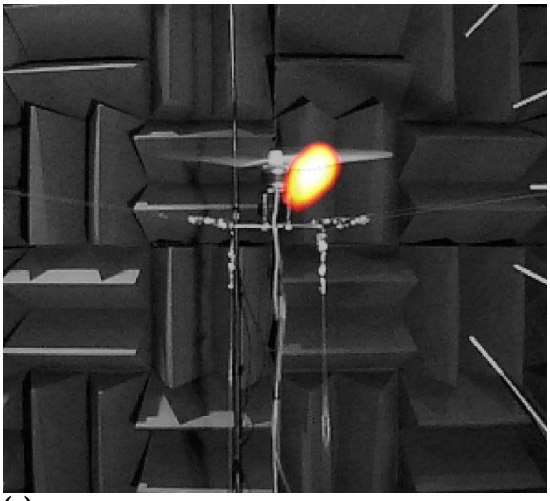

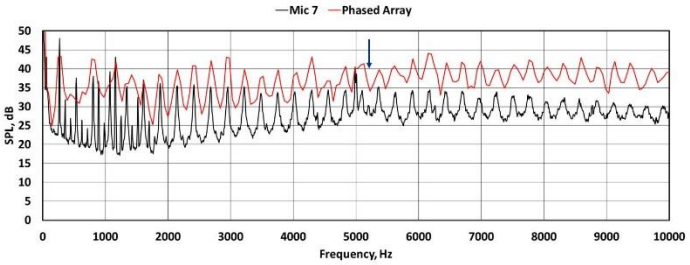

(e) **(f)**

Figure 31. Phased array data for 2312 motor, 5370 RPM, 5224 Hz (blue arrow in SPL). (a) Beamform image for motor only. (b) SPL for motor only. (c) Beamform image for 2-bladed propeller. (d) SPL for 2-bladed propeller. (e) Beamform image for 3-bladed propeller. (f) SPL for 3-bladed propeller.

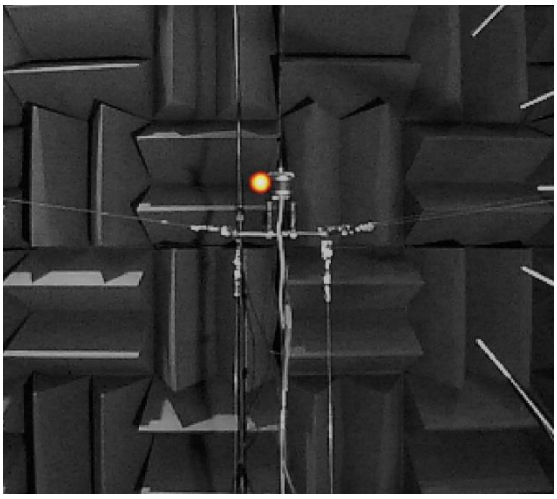

(a)

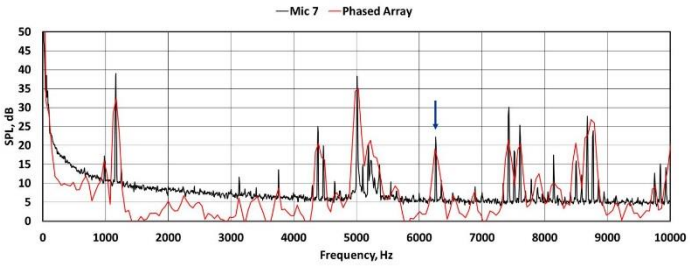

(b)

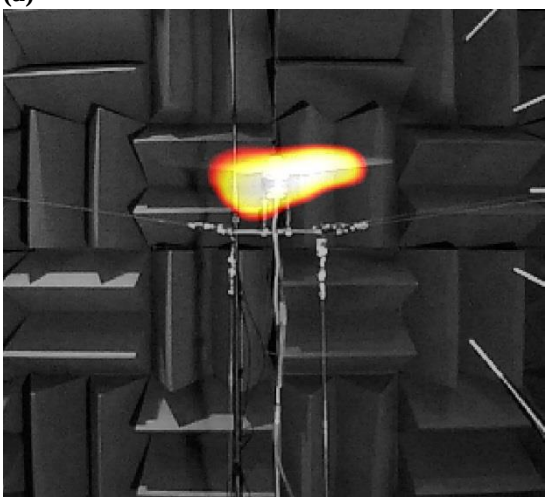

(c)

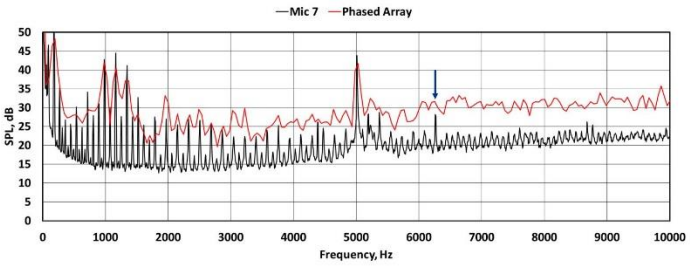

(d)

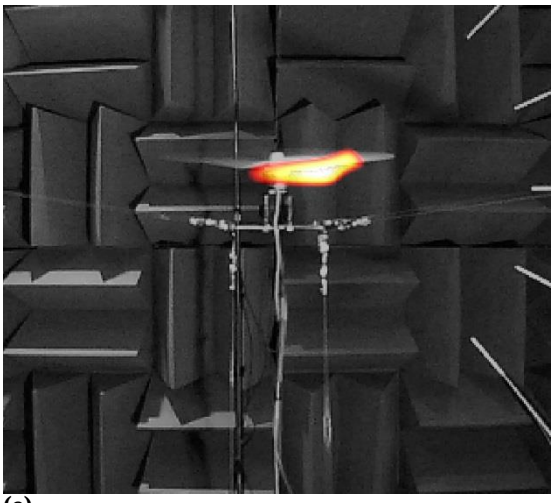

(e)

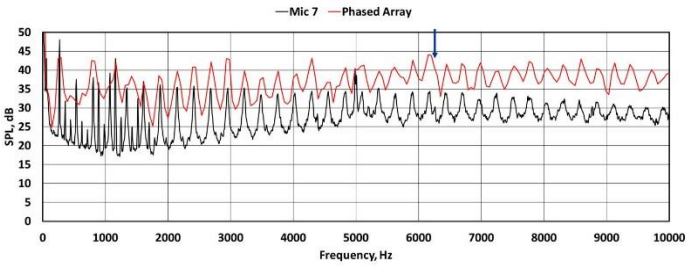

(f)

Figure 32. Phased array data for 2312 motor, 5370 RPM, 6250 Hz (blue arrow in SPL). (a) Beamform image for motor only. (b) SPL for motor only. (c) Beamform image for 2-bladed propeller. (d) SPL for 2-bladed propeller. (e) Beamform image for 3-bladed propeller. (f) SPL for 3-bladed propeller.

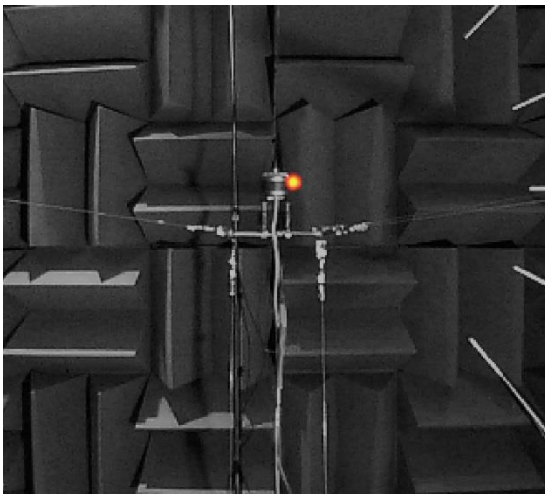

(a)

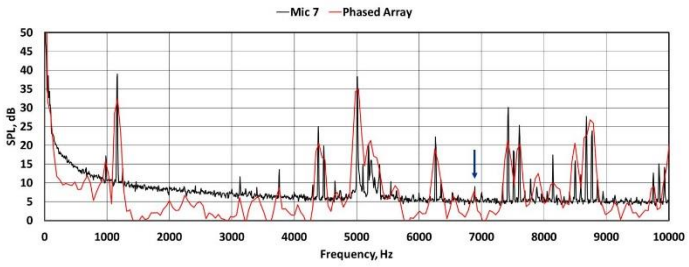

(b)

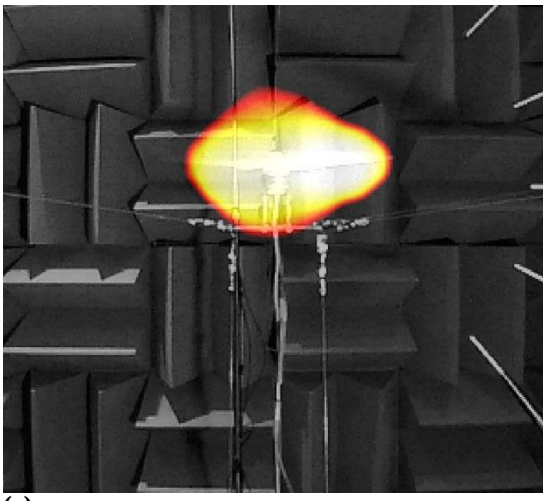

(c)

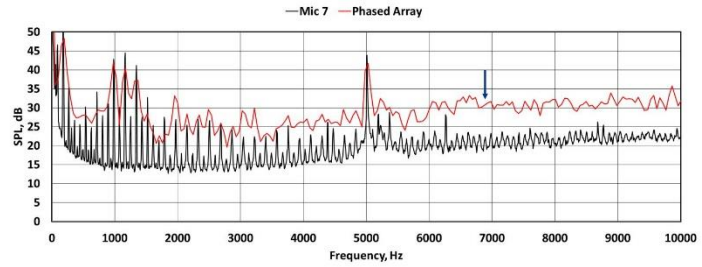

(d)

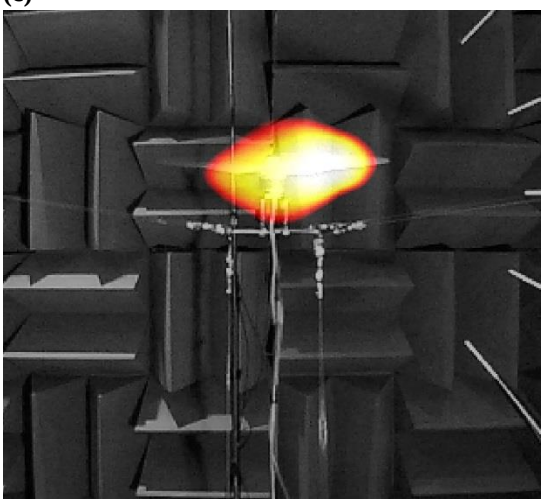

(e)

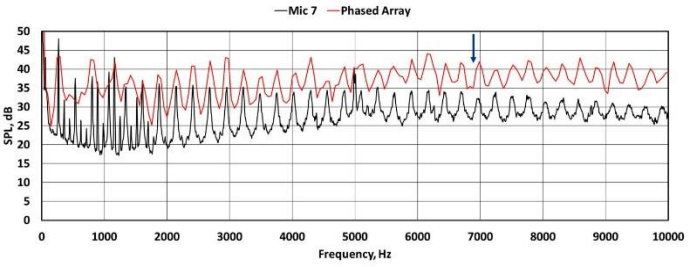

(f)

Figure 33. Phased array data for 2312 motor, 5370 RPM, 6885 Hz (blue arrow in SPL). (a) Beamform image for motor only. (b) SPL for motor only. (c) Beamform image for 2-bladed propeller. (d) SPL for 2-bladed propeller. (e) Beamform image for 3-bladed propeller. (f) SPL for 3-bladed propeller.

IV. Conclusion

Tests were conducted on motors used for small quadcopters to study the acoustic characteristics. The motors were tethered in an anechoic chamber to isolate the noise contributions from the motor. Comparisons were made with and without a propeller loading source over several speeds. The following conclusions are made from the investigation:

- The most important noise source are tones, but there can be broadband noise as a secondary source over a narrow frequency range that is dependent on the type of motor.
- Motor noise peaks in a direction normal to the motor rotor axis and falls off above and below the motor at other angles.
- Relative to motor only tests, adding the propeller introduces shaft order tones, blade passing frequency tones, and higher harmonics that are evident up to about 4000 Hz. The propeller also increases the broadband noise across the entire spectra. The directivity of sound reverses the trend from motor only results with peak levels above and below the motor.
- Strong motor tones can be amplified by the propeller loading by 5 to 15 dB and exceed the propeller noise levels. But this was only observed for a two-bladed propeller. A three-bladed propeller showed no amplification of the motor tones.
- The phased microphone array provides acoustic spectra that are in good agreement with far field microphone data. Beamform images successfully distinguish motor and propeller noise contributions. The spatial resolution and apparent variation of source locations on the motor case suggests multiple modes of vibration are responsible for motor tones at different speeds.

Acknowledgments

This work was supported the Revolutionary Vertical Lift Technology (RVLT) project in the Advanced Air Vehicles Program.

References

[1]Amazon Prime Air, https://www.amazon.com/Amazon-Prime-Air/b?node=8037720011 , Accessed Mar. 12, 2018.

[2]Holden, J and Goel, N., "Fast-Forwarding to a Future of On-Demand Urban Air Transportation," UBER Elevate Summit, October 27, 2016. https://www.uber.com/info/elevate/, Accessed Mar. 12, 2018

[3]Zawodny, N., Boyd, D., Jr., and Burley, C., "Acoustic Characterization and Prediction of Representative, Small-Scale Rotary-Wing unmanned Aircraft System Components," 72nd American Helicopter Society International Annual Forum, West Palm Beach, FL, 2016, pp. 34-38.

[4]Intaratep, N., Alexander, W., Devenport, W, Grace, S. and Dropkin, A., "Experimental Study of Quadcopter Acoustics and Performance at Static Thrust Conditions," 22nd AIAA/CEAS Aeroacoustics Conference, AIAA 2016-2873, 2016.

[5]Henderson, B.S., Huff, D.L., Cluts, J.D. and Ruggeri, C.R., "Electric Motor Noise from Small Quadcopters: Part II - Source Characteristics and Predictions," 28th AIAA/CEAS Aeroacoustics Conference, 2018.

[6]Dougherty, R., "BeamformX Reference Manual," Version 3, May 6, 2017, https://www.optinav.com/beamformx-aeroacoustic-detector , Accessed Mar. 12, 2018.